Supplementary Information

1. Abbreviations

ZA hydrogel, hydrogel formed by Zn^{2+} cross-linked sodium alginate; SA, sodium alginate; HPDA, hollow polydopamine nanoparticles; $Re_{RL\text{-}QN15}$, reduced structure of RL-QN15; $Li_{RL\text{-}QN15}$, linear structure of RL-QN15 without disulfide bonds; HPDAlCy$_{RL\text{-}QN15}$/ZA hydrogel, ZA hydrogel containing HPDA nanoparticles loaded with $Cy_{RL\text{-}QN15}$; rh-bFGF, recombinant human basic fibroblast growth factor; MTS, metallothioneins; FBS, fetal bovine serum; DMEM, Dulbecco's Modified Eagle Medium; PBS, phosphate-buffered saline; HaCaT, human keratinocytes; HSF, human skin fibroblast; HUVECs human umbilical vein endothelial cells; FTIR, Fourier transform infrared spectroscopy; TEM, transmission electron microscopy; XPS, X-ray photoelectron spectroscopy; Calcein-AM, calcein acetoxymethyl; PI, propidium iodide; $ABTS^{+}$, 2,2'azino-bis(3-ethylbenzothiazoline-6-sulfonic acid); DPPH, 2,2-diphenyl-1-picrylhydrazyl; VC, vitamin C; DCFH-DA, 2,7-dichlorofluorescein diacetate; ROS, reactive oxygen species; LPS, lipopolysaccharide; STZ, streptozotocin; H&E, hematoxylin and eosin; PAS, periodic acid-Schiff, TGF-β1, transforming growth factor-β1; TNF-α, tumor necrosis factor; IL-1β, interleukin-1β; IL-10, interleukin-10; VEGF, vascular endothelial growth factor; α-SMA, α-smooth muscle actin; CD31, platelet endothelial cell adhesion molecule; COL I, collagen type I; COL III, collagen type III; INOS, inducible nitric oxide synthase; ARG, arginase; DAB, diaminobenzidine; OCT, optimal cutting temperature; DAPI, 4',6-diamidino-2-phenylindole; IOD, integrated optical densities; HRP, horseradish peroxidase; ELISA, enzyme-linked immunosorbent assay.

2. Materials and Methods

2.1 Chemicals and reagents

All chemical reagents were of analytical grade and used as received unless otherwise noted. The SA (32–250 kD) was obtained from Meyer Co. Ltd. (Shanghai, China). The $ZnCl_2$ was

obtained from Tianjin Chemical Reagent Plant No. 3 (China). Anhydrous ethanol and trichloromethane were purchased from the Sinopharm Chemical Reagent Company (China).

2.2 Keratinocyte scratch healing assay

Human epidermal keratinocytes (HaCaT cells) were cultured in 24-well plates (2×10^5 cells/well) to confluency and cell scratch wounds were modeled using sterile 200-μL pipette tips. The pro-healing effects of Vehicle (phosphate-buffered saline, PBS), positive control (recombinant human basic fibroblast growth factor, rh-bFGF, 100 ng/mL), RL-QN15 (1 nM), $Re_{RL\text{-}QN15}$ (1 nM), $Li_{RL\text{-}QN15}$ (1 nM), $Cy_{RL\text{-}QN15}$ (1 nM), ZA, HPDA, HPDA/ZA, $Cy_{RL\text{-}QN15}$/ZA, HPDAlCy$_{RL\text{-}QN15}$, and HPDAlCy$_{RL\text{-}QN15}$/ZA hydrogels ($ZnCl_2$: 0.0002% w/v, NA: 0.024% w/v, HPDA 0.01 mg/mL, $Cy_{RL\text{-}QN15}$ 1 nM) on the HaCaT cell scratches were determined following previous research [1].

2.3 Effects of RL-QN15-modified peptides on full-thickness skin wounds in mice

Briefly, two 10-mm diameter full-thickness wounds were created on the dorsal skin of male Kunming mice using a biopsy puncture device. The wounds were treated with PBS (Vehicle), positive control (rh-bFGF, 100 ng/mL), and 1 nM of RL-QN15, $Re_{RL\text{-}QN15}$, $Li_{RL\text{-}QN15}$, and $Cy_{RL\text{-}QN15}$ (20 μL twice daily), respectively. Wound status and area were measured using ImageJ software. Wound repair rates were calculated according to an earlier study [2].

2.4 Preparation and characterization of HPDAlCy$_{RL\text{-}QN15}$/ZA hydrogel

The HPDAlCy$_{RL\text{-}QN15}$/ZA hydrogel was prepared. First, HPDA nanoparticles were obtained from our previous study [2]. HPDA was dissolved in PBS by ultrasonication (VCX750, Nanjing Biotechnology Co. Ltd., China) to prepare the HPDA solution at a concentration of 0.01 mg/mL. The ZA hydrogel (Zn^{2+} cross-linked sodium alginate) was prepared following previous study, with some modification [3]. Briefly, SA (2.4% w/v) was added into ddH_2O and cross-linked in $ZnCl_2$ solution (0.002% w/v). To prepare HPDAlCy$_{RL\text{-}QN15}$ solution, HPDA was mixed with $Cy_{RL\text{-}QN15}$ (1 nM) and shaken at 4 ℃ for 18 h to adequately load $Cy_{RL\text{-}QN15}$ into

HPDA. After centrifugation (10 000 × *g*, 5 min, 4 °C), the supernatant was discarded, and the precipitates were resuspended in PBS to obtain HPDAlCy$_{RL\text{-}QN15}$ solution. Finally, the HPDA/ZA, Cy$_{RL\text{-}QN15}$/ZA and HPDAlCy$_{RL\text{-}QN15}$/ZA hydrogels were obtained by mixing ZA with HPDA, Cy$_{RL\text{-}QN15}$, and HPDAlCy$_{RL\text{-}QN15}$, respectively, followed by uniform stirring with an electric stirrer at 300 rpm (25 °C, 12 h). The hydrogel samples were then freeze-dried in a vacuum refrigeration drier (LGJ-10, Beijing, China) until further use. The effects of Zn^{2+} on the formation of the HPDAlCy$_{RL\text{-}QN15}$/ZA hydrogel was determined based on previous study [4].

The hydrogels were characterized using transmission electron microscopy (TEM, FEI, TECNAI G2, F30, USA), Fourier transform infrared spectroscopy (FTIR, NICOLET-IS10, Thermo Scientific, USA), scanning electron microscopy (SEM, SU8020, Hitachi, Japan), and X-ray photoelectron spectroscopy (XPS, K-alpha XPS spectrometer, Thermo Fisher Scientific, USA). The compression properties of all samples were examined on a universal tensile tester (CMT 6103, Instron, USA) at a rate of 2 mm/min, based on previous study [5]. Hydrogels rheology were measured on a TA rheometer (Haake Mars 60, Germany) according to previous study [6].

Porosity of the ZA and HPDAlCy$_{RL\text{-}QN15}$/ZA hydrogels were detected by anhydrous ethanol replacement according to previous study [3]. Briefly, the lyophilized samples were immersed in a volume of ethanol in a graduated measuring cylinder for 10 min. Porosity of the ZA and HPDAlCy$_{RL\text{-}QN15}$/ZA hydrogels were calculated based on the change in the volume of hydrogel soaked in ethanol.

The swelling ratio of the ZA and HPDAlCy$_{RL\text{-}QN15}$/ZA hydrogels was measured according to previous studies [7,8]. Dry weight (Wd) of the freeze-dried specimens was measured. The lyophilized samples were then immersed in DMEM solution at 37 °C. The hydrogels were collected at different time points and weighed (Wt) separately. The swelling ratio (SR) was calculated using the following equation: $SR = (Wt - Wd) / Wd$.

2.5 Biocompatibility and degradation of HPDAlCy$_{RL-QN15}$/ZA hydrogel

2.5.1 *In vitro* toxicity

Toxicity of the HPDAlCy$_{RL-QN15}$/ZA hydrogel in HaCaT cells was analyzed using the live/dead cell viability assay [1]. Briefly, HaCaT cells (2×10^5 cells/well) were cultured in a 12-well plate and incubated with Vehicle (PBS), ZA, HPDA, Cy$_{RL-QN15}$, HPDA/ZA, Cy$_{RL-QN15}$/ZA, HPDAlCy$_{RL-QN15}$, and HPDAlCy$_{RL-QN15}$/ZA hydrogel for 12 h at 37 °C, respectively. A calcein acetoxymethyl/propidium iodide (calcein-AM/PI) double staining kit (Beyotime, Shanghai, China) was used according to the protocols provided by the manufacturer. The stained HaCaT cells were imaged and analyzed by confocal laser scanning fluorescence microscopy (Axio Observer Z1, Zeiss, Germany).

2.5.2 *In vivo* toxicity

Toxicity of the HPDAlCy$_{RL-QN15}$/ZA hydrogel was evaluated in C57BL/6 mice with full-thickness skin wounds following previous study [2]. Briefly, wounds were treated twice a day with Vehicle (PBS), ZA, HPDA, Cy$_{RL-QN15}$, HPDA/ZA, Cy$_{RL-QN15}$/ZA, HPDAlCy$_{RL-QN15}$, and HPDAlCy$_{RL-QN15}$/ZA hydrogel ($ZnCl_2$: 0.02% w/v, NA 2.4% w/v, HPDA 0.1 mg/mL, Cy$_{RL-QN15}$ 1 nM), respectively. After 14 days of continuous treatment, major organs (heart, liver, liver, spleen, left lung, and left kidney) were collected for hematoxylin and eosin (H&E) staining and photographed under a light microscope (Zeiss, Primovert, Germany).

2.5.3 Degradation of HPDAlCy$_{RL-QN15}$/ZA hydrogel *in vitro* and *in vivo*

The hydrogels (ZA, HPDA/ZA, Cy$_{RL-QN15}$/ZA, and HPDAlCy$_{RL-QN15}$/ZA) were first resuspended in 5 mL of hyaluronidase and collagenase solution (100 U/mL), incubated in a horizontal shaker at 37 °C, and collected at various time points and lyophilized. The weights of the remaining gels were calculated using the following formula:

$$\text{Weight remaining (\%)} = W0 / Wt \times 100$$

where W0 and Wt are the weights of the hydrogels before and after immersion in

hyaluronidase and collagenase solution, respectively. The experiment was repeated three times for all samples, (n = 3).

Next, 0.1 mL of hydrogels were injected subcutaneously into the abdomen of Kunming mice, and the degradation status of the hydrogel in mice was observed on days 1 and 14.

2.6 Assessment of cell proliferation

In brief, HaCaT cells, RAW 264.7 cells, human umbilical vein endothelial cells (HUVECs), and human skin fibroblasts (HSFs) were seeded in 96-well plates (5×10^3 cells/well) and incubated with 10 μL of Vehicle (PBS), ZA, HPDA, $Cy_{RL\text{-}QN15}$, HPDA/ZA, $Cy_{RL\text{-}QN15}$/ZA, HPDAl$Cy_{RL\text{-}QN15}$, and HPDAl$Cy_{RL\text{-}QN15}$/ZA for 24 h. The MTS assay (Promega, Madison, WI, USA) was performed to detect cell viability according to the manufacturer's instructions.

2.7 *In vitro* HUVEC migration and tube formation assays

HUVECs (1×10^4 cells/well) were seeded in the upper chamber of a Transwell plate (8 μm, Corning, USA). Vehicle (PBS), $Cy_{RL\text{-}QN15}$, HPDAl$Cy_{RL\text{-}QN15}$, and HPDAl$Cy_{RL\text{-}QN15}$/ZA were added to the culture medium with 1% fetal bovine serum (FBS) in the lower chamber at 37 °C for 24 h. The upper chamber membrane was then stained with crystalline violet (Solarbio, C8470, China) and cell migration was observed using a microscope (Motic, AE2000, China). A tube formation assay was performed using Matrigel basement membrane matrix (356234, Biosciences, San Jose, USA) [9]. Briefly, unfrozen Matrigel was added to a 96-well plate and cultured with Vehicle (PBS), $Cy_{RL\text{-}QN15}$, HPDAl$Cy_{RL\text{-}QN15}$, and HPDAl$Cy_{RL\text{-}QN15}$/ZA at 37 °C for 6 h. Tube formation was observed using a microscope and evaluated through five independent fields.

2.8 Antioxidant activity of HPDAl$Cy_{RL\text{-}QN15}$/ZA hydrogel

The antioxidant activities of the HPDAl$Cy_{RL\text{-}QN15}$/ZA hydrogel was evaluated using 2,2-

benzyl-bis (3-ethylbenzothiazoline-6-sulfonic acid)-diamine salt (ABTS) and 2,2-diphenyl-1-pyridylhydrazine (DPPH) (Sigma-Aldrich, St Louis, MO, USA). The ABTS radical cation ($ABTS^+$) and DPPH/methanol solution were generated based on prior methods [10], and absorbance was measured at 415 nm and 517 nm, respectively. We used ddH_2O and vitamin C (Vc) as a negative and positive control, respectively. The free radical scavenging rate (%) was calculated according to former study [10].

To examine the preservation of oxidative stress of $HPDAlCy_{RL\text{-}QN15}$/ZA hydrogel, 2',7'-dichlorofluorescein diacetate (DCFH-DA) was used to detect the production of reactive oxygen species (ROS). Following previous study [11], HUVECs were incubated with samples and H_2O_2 (1 mM) for 1 h and stained with DCFH-DA (20 μM) for 30 min in the dark. The fluorescence intensity of DCFH-DA was measured by flow cytometry (CyFlow Space, PARTEC, Germany) to assess intracellular ROS intensity.

2.9 Effects **of samples on chronic diabetic skin wounds in mice**

The created 8-mm full-thickness skin wounds were treated with Vehicle (PBS), Tegaderm wound dressing (3M, USA), $Cy_{RL\text{-}QN15}$, $HPDAlCy_{RL\text{-}QN15}$, and $HPDAlCy_{RL\text{-}QN15}$/ZA for two weeks. Wound condition was documented on days 3, 7, and 14 post-operation, and wound repair rates were calculated according to previous study [2]. Wound tissues were collected from mice on days 3, 7, and 14 post-treatment for enzyme-linked immunosorbent assay (ELISA) detection, histological staining, and fluorescent staining, respectively.

2.10 Histological analysis and immunohistochemical and immunofluorescence staining

For immunohistochemical staining, wound tissue sections were embedded with optimal cutting temperature (OCT) compound tissue embedding medium (Sakura Finetek, USA). The frozen sections (10 μm) were then blocked with 5% goat serum albumin for 2 h and incubated with goat anti-mouse interleukin-1β (IL-1β; Affinity, AF5103, China; 1:100), interleukin-10 (IL-10; Affinity, DF6894, China; 1:100), collagen type I (COL I; Cell Signaling Technology,

#72026, USA; 1:200), and collagen type III (COL III) primary antibodies (Affinity, AF0136, China; 1:200) overnight at 4 °C. After treatment with horseradish peroxidase (HRP) secondary antibodies (Abcam, USA; 1:400) for 1 h, the sections were colored using a diaminobenzidine (DAB) kit (Zhongshan JinQiao Biotech; ZLI-9018) and stained with hematoxylin. Quantitative analysis was conducted according to previous study [12].

For immunofluorescence staining, cryosections were incubated with rabbit anti-mouse CD31 (Affinity AF0077, China; 1:200), vascular endothelial growth factor (VEGF) (Abcam, ab233693, USA; 1:500), α-smooth muscle actin (α-SMA) (Cell Signaling Technology, #19245, USA; 1:200), and Ki67 primary antibodies (Cell Signaling Technology, #12075, USA; 1:50) overnight at 4 °C, then incubated with goat anti-rabbit IgG Alexa Fluor ® 488 and DAPI (Sigma, F6057, USA) to visualize nuclei. To confirm the polarization of macrophages, the cryosections were incubated with rat anti-mouse F4/80 (Abcam, ab6640, USA; 1:100), rabbit anti-mouse, inducible nitric oxide synthase (INOS) (Abcam, ab178945, USA; 1:300), and arginase (ARG) antibodies (Affinity, DF6657, China; 1:200) for restaining, respectively. The sections were then incubated with goat anti-rabbit IgG Alexa Fluor ® 488 and goat anti-rat IgG Alexa Fluor ® 647 (Abcam, ab150159, USA; 1:200) for 1 h at 37 °C, with DAPI used to visualize nuclei. Fluorescence images were recorded using confocal laser scanning microscopy. Quantitative analysis was conducted according to previous study [13].

2.11 Human *ex vivo* diabetic skin wound model

Skin sample donations were obtained from diabetic patients undergoing amputation surgeries (age range = 49–62 years) (Table S1). The skin specimens were divided into 6-mm diameter samples using a biopsy tool and a 2-mm diameter *ex vivo* diabetic full-thickness skin wound was created in the center of each specimen. The skin explants were cultured in 6-well plates with 1.5 × 1.5-cm sterile gauze and DMEM/high glucose medium supplemented with 10% FBS and 1% double antibodies, with the skin epidermis and wound exposed to air in a 5%

CO_2 humidified atmosphere at 37 °C. Vehicle (PBS), $Cy_{RL\text{-}QN15}$, $HPDAlCy_{RL\text{-}QN15}$, and $HPDAlCy_{RL\text{-}QN15}$/ZA were applied (10 μL) to wounds once a day, respectively, and the medium was changed every two days.

After one week of culture, the *ex vivo* diabetic full-thickness skin wound tissues were extracted and examined for tumor necrosis factor-α (TNF-α) and transforming growth factor-β1 (TGF-β1) levels using ELISA kits; paraffin-embedded tissues for H&E, Masson trichrome, and PAS staining; and immunofluorescence staining for CD31 and α-SMA expression levels, respectively.

2.12 Statistical analysis

All data were expressed as mean ± standard deviation (SD) and analyzed using GraphPad Prism v7.0 (LaJolla, CA, USA). Student's *t*-test and one-way analysis of variance (ANOVA) with Tukey's multiple comparison test were used for comparative analysis. Statistical significance was expressed as **** $P < 0.0001$, *** $P < 0.001$, ** $P < 0.01$, and * $P < 0.05$, respectively. All experiments were performed with at least three independent experiments in triplicate.

3. Supplementary Results

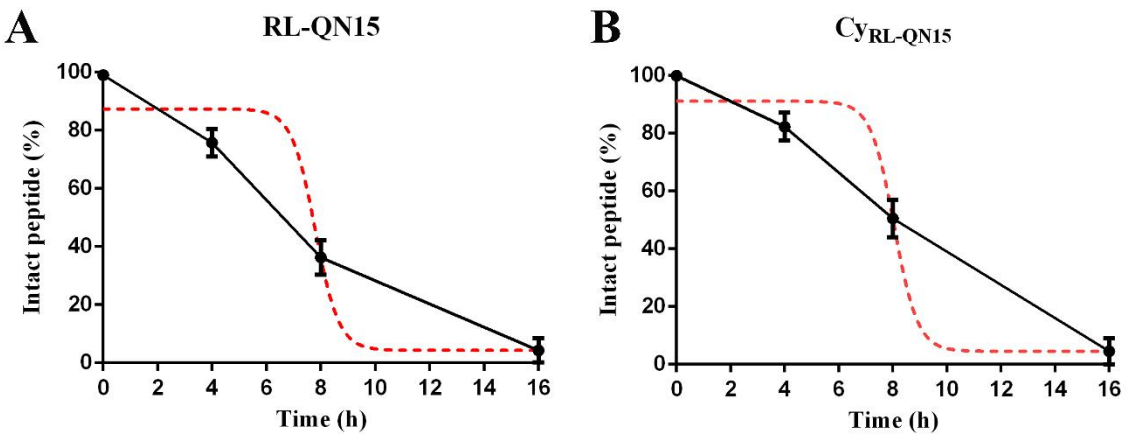

Figure S1. Stability of RL-QN15 and Cy$_{RL-QN15}$ in plasma.

A. Half-life of RL-QN15 in plasma (7.64 h).

B. Half-life of Cy$_{RL-QN15}$ in plasma (8.15 h).

Figure S2. Zn^{2+} promoted formation of HPDAlCy$_{RL-QN15}$/ZA hydrogel with greater cross-linking than SA and ZA.

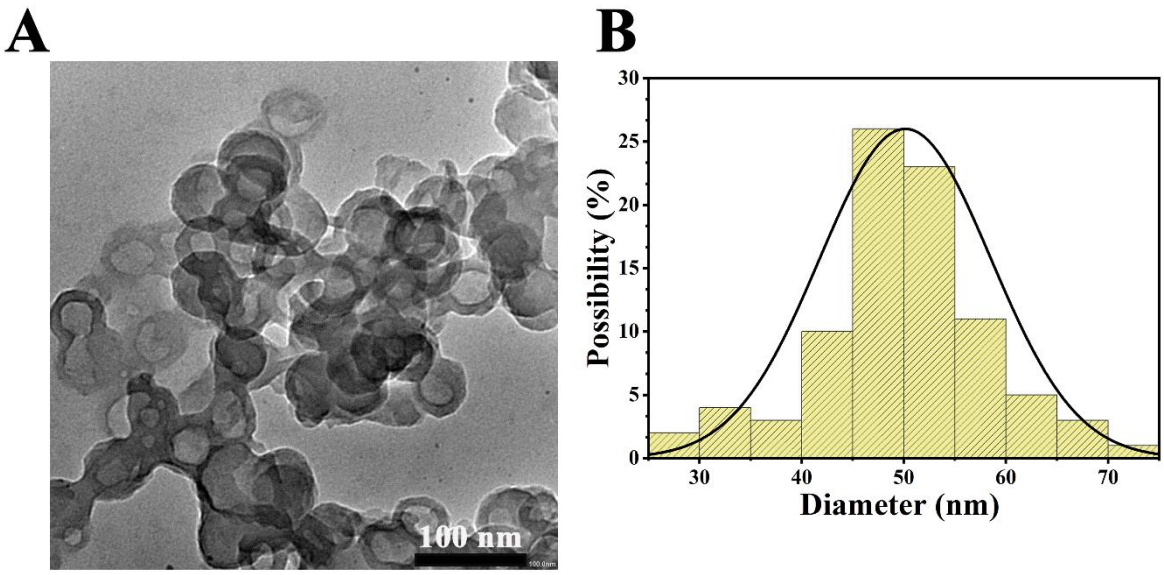

Figure S3. Transmission electron microscopy of HPDA nanoparticles.

A. Transmission electron microscopy of HPDA pores. Scale bar (100 nm) is indicated by a line.

B. Grain size distribution of HPDA, n = 88.

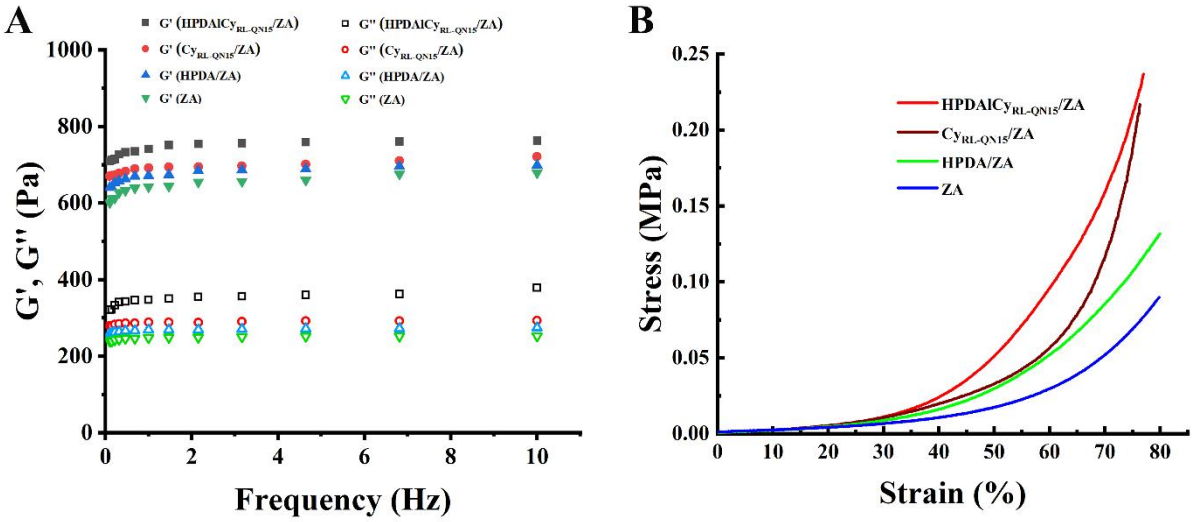

Figure S4. Mechanical properties and stability of hydrogels.

A. Rheology of ZA, HPDA/ZA, Cy$_{RL-QN15}$/ZA, and HPDAlCy$_{RL-QN15}$/ZA hydrogels were measured in frequency range of 0 to 10 Hz at 37 °C.

B. Compressive strain-stress curve of ZA, HPDA/ZA, Cy$_{RL-QN15}$/ZA, and HPDAlCy$_{RL-QN15}$/ZA

hydrogels.

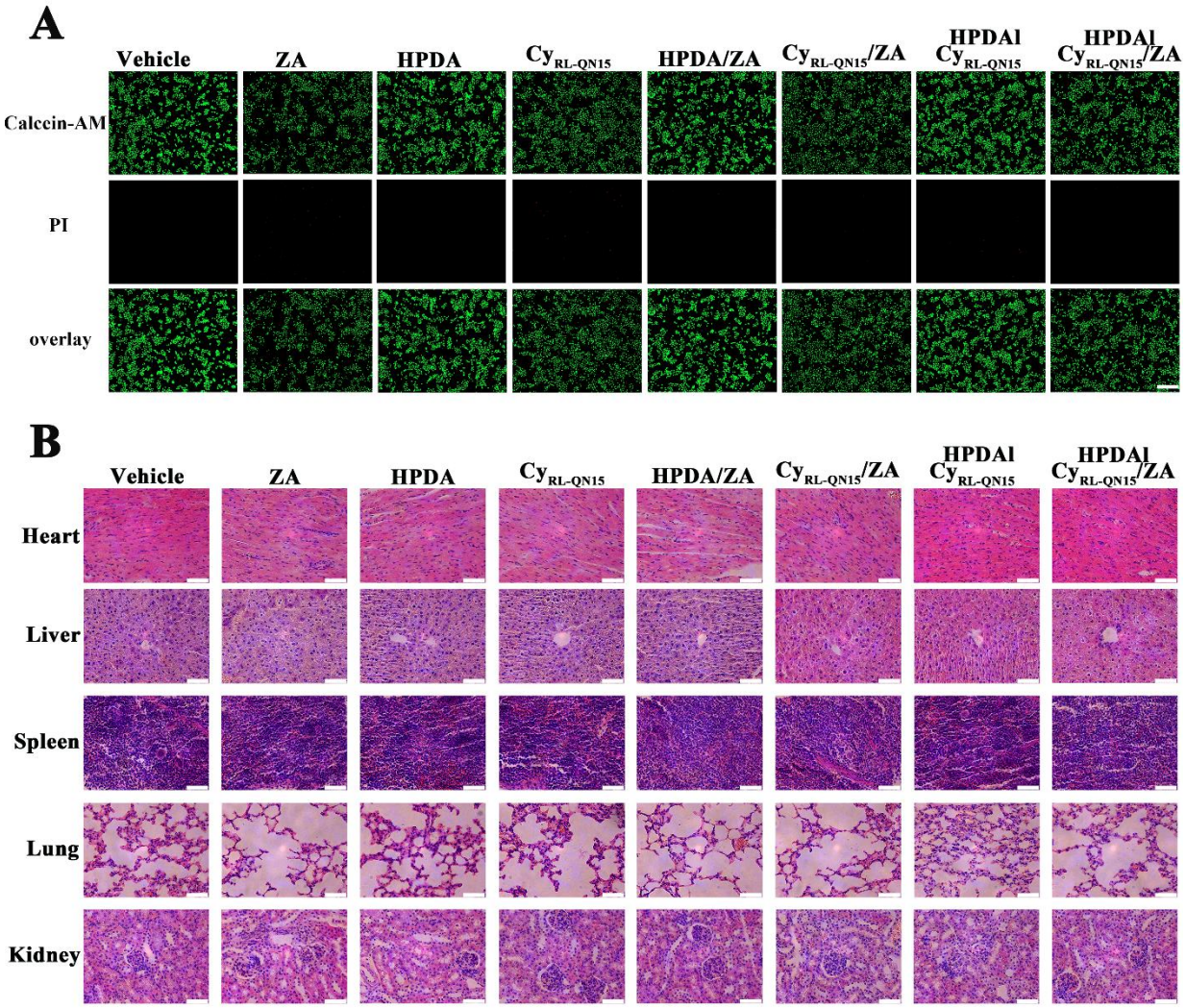

Figure S5. *In vitro* and *vivo* biocompatibility testing.

A. *In vitro* biocompatibility assay of HaCaT cells treated with Vehicle (serum-free medium), ZA, HPDA, $Cy_{RL\text{-}QN15}$, HPDA/ZA, $Cy_{RL\text{-}QN15}$/ZA, HPDAl$Cy_{RL\text{-}QN15}$, and HPDAl$Cy_{RL\text{-}QN15}$/ZA. Representative confocal fluorescence images of cells stained with calcein-AM and PI. Scale bar: 75 μm.

B. H&E staining of major organs in mice with full-thickness skin wounds treated with different samples. Scale bar: 100 μm.

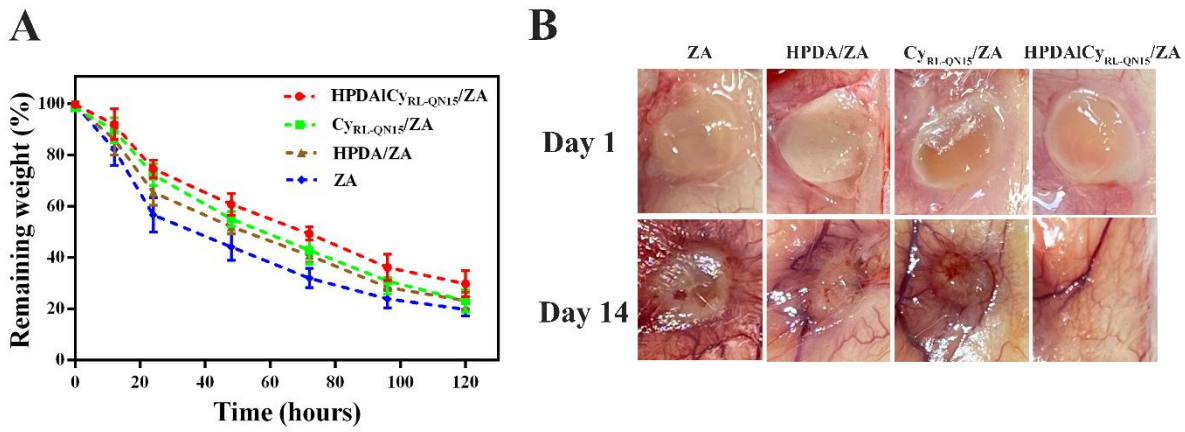

Figure S6. Degradation of ZA, HPDA/ZA, Cy$_{RL-QN15}$/ZA, and HPDAlCy$_{RL-QN15}$/ZA hydrogels *in vitro* and *in vivo*.

A. Degradation of ZA, HPDA/ZA, Cy$_{RL-QN15}$/ZA, and HPDAlCy$_{RL-QN15}$/ZA hydrogels under hyaluronidase and collagenase solution (100 U/mL) treatment at different incubation times at 37 °C.

B. Subcutaneous degradation of ZA, HPDA/ZA, Cy$_{RL-QN15}$/ZA, and HPDAlCy$_{RL-QN15}$/ZA hydrogels in mouse abdomen on days 1 and 14.

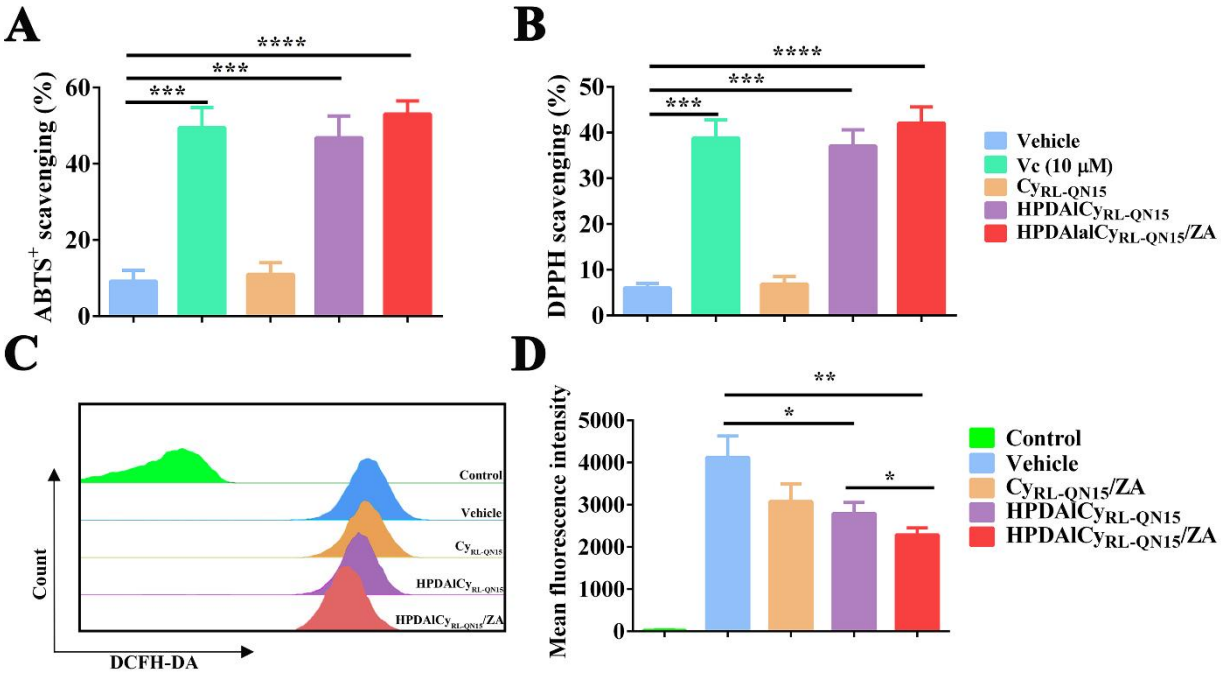

Figure S7. Antioxidant capacity of HPDAlCy$_{RL-QN15}$/ZA hydrogel *in vitro*.

A-B. Effects of samples on scavenging $ABTS^+$ and DPPH free radicals.

C. ROS content in HUVEC cells following H_2O_2 stimulation assessed by flow cytometry and staining with ROS-specific probe 2,7-dichlorodihydrofluorescein diacetate (DCFH-DA), Control group received no treatment.

D. Quantification of average fluorescence intensity.

Data are mean ± SD, generated from three independent experiments performed in triplicate. *, **, ***, and **** indicate $P < 0.05$, $P < 0.01$, $P < 0.001$, and $P < 0.0001$, respectively.

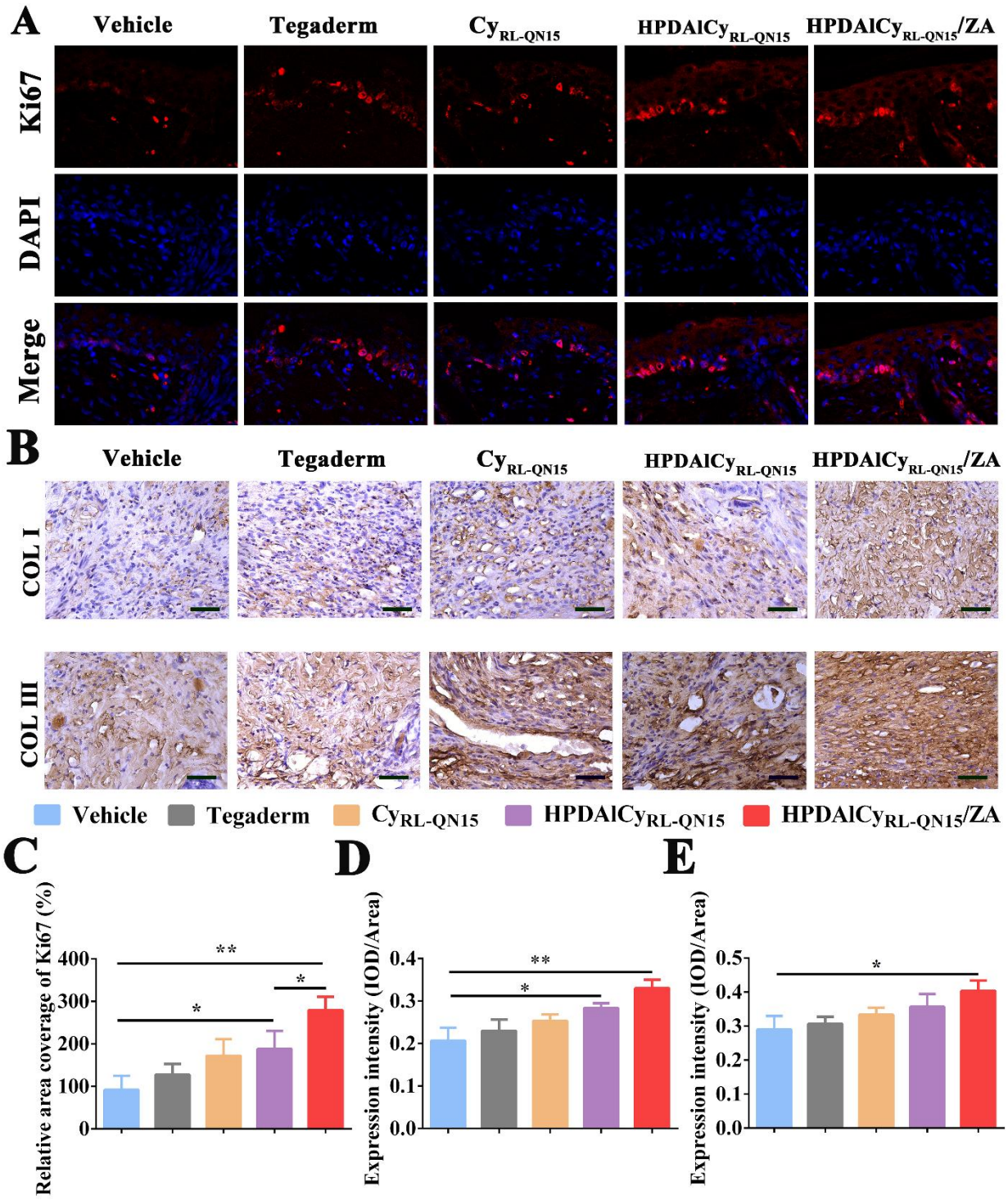

Figure S8. Expression of Ki67 by immunofluorescence staining and COL I and COL III deposition in skin tissue.

A. Representative images of immunofluorescence staining of Ki67 on day 14 after treatment. Scale bar: 50 μm.

B. Representative graph of COL I and COL III immunohistochemical staining. Scale bar: 75

μm.

C. Quantification data of Ki67 in wounds.

D-E. Quantification of positive COL I and COL III immunohistochemical staining, respectively. Data are mean ± SD, generated from three independent experiments performed in triplicate. * and ** indicate $P < 0.05$ and $P < 0.01$, respectively.

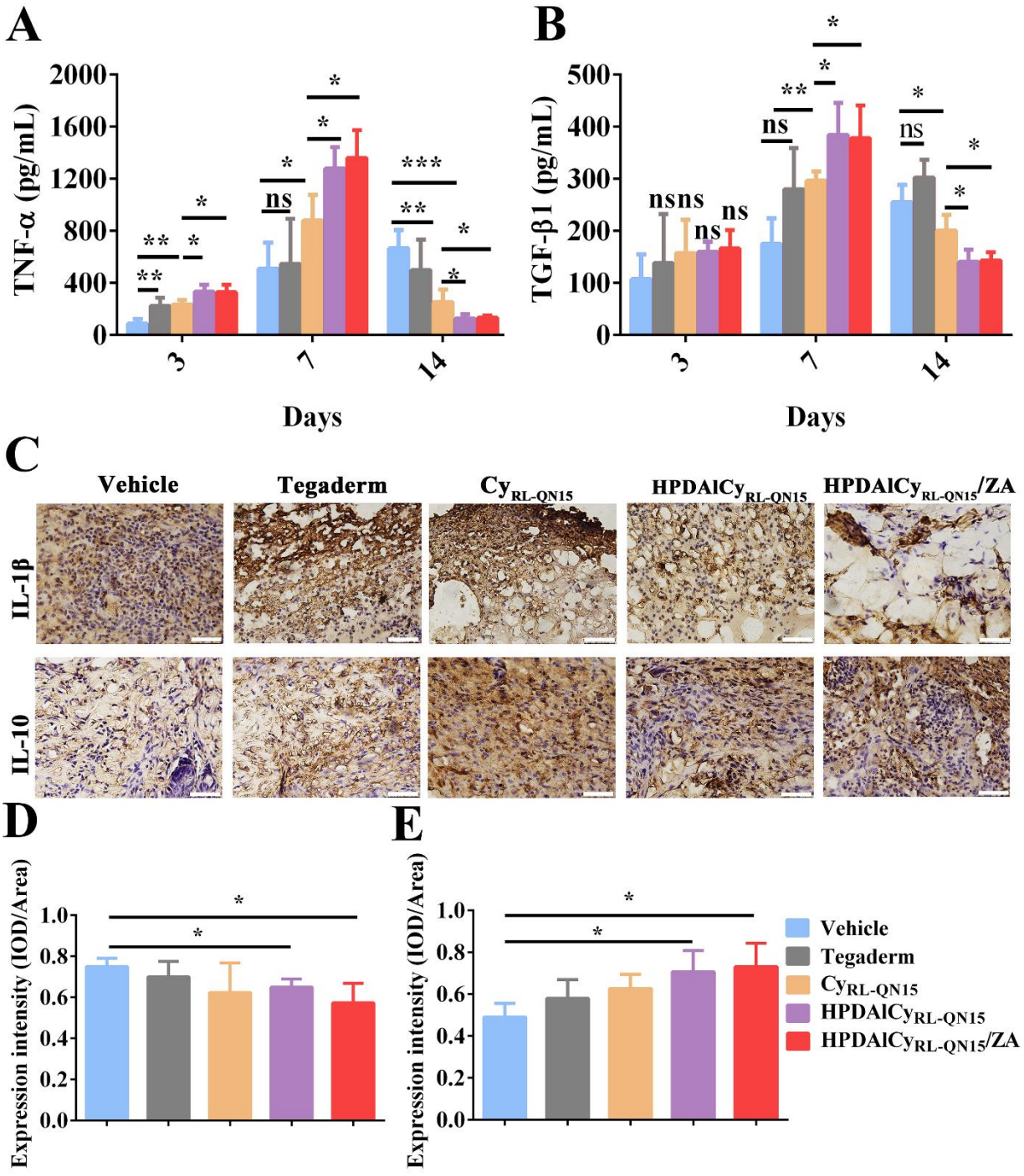

Figure S9. TNF-α, TGF-β1, IL-1β, and IL-10 expression levels in skin wound tissues from type 2 diabetic mice.

A-B. TNF-α and TGF-β1 expression levels in mouse skin wound tissues on days 3, 7, and 14.

C. Representative graph of IL-1β and IL-10 immunohistochemical staining of skin wound tissues of type 2 diabetic mice on day 7. Scale bar: 75 μm.

D-E. Quantification of intensity of IL-1β- and IL-10-positive staining, respectively.

Data are mean ± SD, generated from three independent experiments performed in triplicate. ns, no significance; *, **, and *** indicate $P < 0.05$, $P < 0.01$, and $P < 0.001$, respectively.

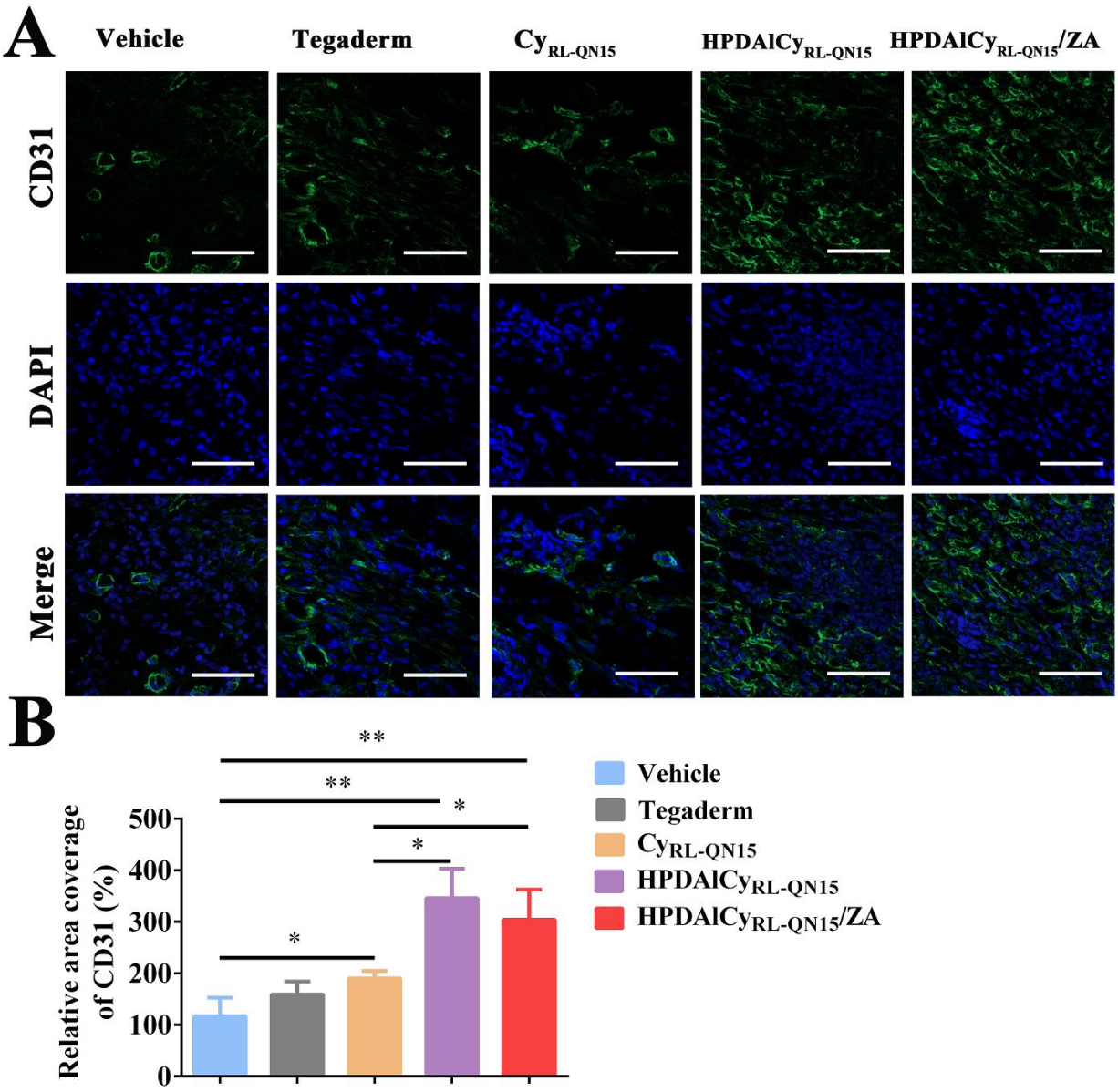

Figure S10. Immunofluorescence staining of CD31 in skin wounds of type 2 diabetic mice.

A. Representative images of immunofluorescence staining of CD31 in mouse skin wounds on day 14 after treatment. Scale bar: 50 μm.

B. Quantification data of CD31 in wounds. Data are mean ± SD, generated from three independent experiments performed in triplicate. * and ** indicate $P < 0.05$ and $P < 0.01$, respectively.

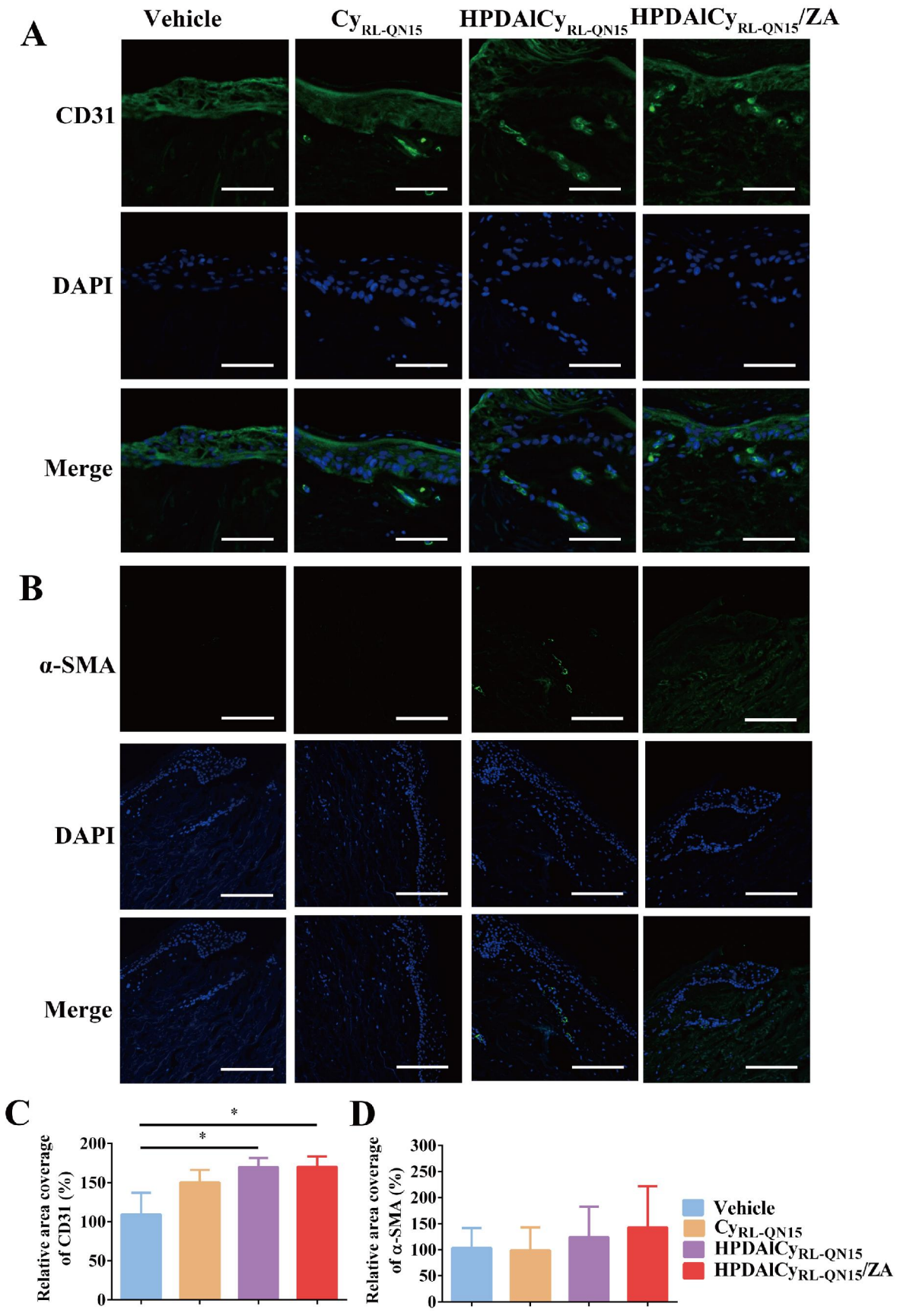

Figure S11. HPDAlCy$_{RL\text{-}QN15}$/ZA hydrogel promoted angiogenesis in *ex vivo* diabetic skin

wounds.

A-B. Representative images of CD31 and α-SMA immunofluorescence staining on day 7 of *ex vivo* skin culture treatment.

C-D. Quantification of positive stains for CD31 and α-SMA. Data are mean ± SD, generated from three independent experiments performed in triplicate, * indicate $P < 0.05$.

Table 1. Characteristics of patients

Patient	Age (years)	Sex	Location
Patient 1	62	Female	Left second toe
Patient 2	49	Female	Right leg
Patient 3	54	Male	Right first toe

References

1 Qin, P. *et al.* Zn(2+) Cross-Linked Alginate Carrying Hollow Silica Nanoparticles Loaded with RL-QN15 Peptides Provides Promising Treatment for Chronic Skin Wounds. *ACS applied materials & interfaces* **14**, 29491-29505, doi:10.1021/acsami.2c03583 (2022).

2 Sun, H. *et al.* Hollow polydopamine nanoparticles loading with peptide RL-QN15: a new pro-regenerative therapeutic agent for skin wounds. *Journal of nanobiotechnology* **19**, 304, doi:10.1186/s12951-021-01049-2 (2021).

3 Zheng, Z. *et al.* A cannabidiol-containing alginate based hydrogel as novel multifunctional wound dressing for promoting wound healing. *Biomaterials advances* **134**, 112560, doi:10.1016/j.msec.2021.112560 (2022).

4 Qian, Y. *et al.* Immunoregulation in Diabetic Wound Repair with a Photoenhanced Glycyrrhizic Acid Hydrogel Scaffold. *Advanced materials (Deerfield Beach, Fla.)* **34**, e2200521, doi:10.1002/adma.202200521 (2022).

5 Xie, H. *et al.* Biocompatible, antibacterial and anti-inflammatory zinc ion cross-linked quaternized cellulose-sodium alginate composite sponges for accelerated wound healing. *International journal of biological macromolecules* **191**, 27-39, doi:10.1016/j.ijbiomac.2021.09.047 (2021).

6 Chen, X. *et al.* Preparation and Application of Quaternized Chitosan- and AgNPs-Base Synergistic Antibacterial Hydrogel for Burn Wound Healing. *Molecules (Basel, Switzerland)* **26**, doi:10.3390/molecules26134037 (2021).

7 Li, C., Wang, J., Zhao, M., Zhang, S. & Zhang, Y. Toll-like receptor 4 antagonist FP7

alleviates lipopolysaccharide–induced septic shock via NF–kB signaling pathway. *Chemical biology & drug design* **97**, 1151–1157, doi:10.1111/cbdd.13837 (2021).

8 Zhang, M. *et al.* Alginate–chitosan oligosaccharide–ZnO composite hydrogel for accelerating wound healing. *Carbohydrate polymers* **266**, 118100, doi:10.1016/j.carbpol.2021.118100 (2021).

9 Wu, D. *et al.* Exosomes Derived from Bone Mesenchymal Stem Cells with the Stimulation of Fe(3)O(4) Nanoparticles and Static Magnetic Field Enhance Wound Healing Through Upregulated miR–21–5p. *International journal of nanomedicine* **15**, 7979–7993, doi:10.2147/ijn.S275650 (2020).

10 Xie, C. *et al.* Novel amphibian–derived antioxidant peptide protects skin against ultraviolet irradiation damage. *J Photochem Photobiol B* **224**, 112327, doi:10.1016/j.jphotobiol.2021.112327 (2021).

11 Liu, J. *et al.* Dihydroartemisinin Induces Endothelial Cell Autophagy through Suppression of the Akt/mTOR Pathway. *J Cancer* **10**, 6057–6064, doi:10.7150/jca.33704 (2019).

12 Fan, Y. *et al.* Dual–target MDM2/MDMX inhibitor increases the sensitization of doxorubicin and inhibits migration and invasion abilities of triple–negative breast cancer cells through activation of TAB1/TAK1/p38 MAPK pathway. *Cancer Biol Ther* **20**, 617–632, doi:10.1080/15384047.2018.1539290 (2019).

13 Tu, Z. *et al.* Engineering Bioactive M2 Macrophage–Polarized Anti–Inflammatory, Antioxidant, and Antibacterial Scaffolds for Rapid Angiogenesis and Diabetic Wound Repair. *Advanced Functional Materials* **31**, 2100924, doi:https://doi.org/10.1002/adfm.202100924 (2021).